J|A|C|S
ARTICLES
Published on Web 05/24/2002

Epitaxial Growth and Photochemical Annealing of Graded CdS/ZnS Shells on Colloidal CdSe Nanorods

Liberato Manna, Erik C. Scher, Liang-Shi Li, and A. Paul Alivisatos*

Contribution from the Department of Chemistry, University of California, Berkeley and Materials Sciences Division, Lawrence Berkeley National Laboratory, Berkeley, California 94720

Received February 15, 2002

Abstract: We report the preparation and structural characterization of core/shell CdSe/CdS/ZnS nanorods. A graded shell of larger band gap is grown around CdSe rods using trioctylphosphine oxide as a surfactant. Interfacial segregation is used to preferentially deposit CdS near the core, providing relaxation of the strain at the core/shell interface. The reported synthesis allows for variation of the shell thickness between one and six monolayers, on core nanorods ranging from aspect ratios of 2:1 to 10:1. After an irreversible photochemical annealing process, the core/shell nanorods have increased quantum efficiencies and are stable in air under visible or UV excitation. In addition to their robust optical properties, these samples provide an opportunity for the study of the evolution of epitaxial strain as the shape of the core varies from nearly spherical to nearly cylindrical.

Introduction

Research on colloidal semiconductor nanocrystals is an important field in modern nanoscale science and technology.[1−6] Among the various materials, colloidal CdSe quantum dots are undoubtedly the most studied, due to their tunable emission in the visible range, the advances in their preparation, and their potential use in industrial and biomedical applications.[7−13]

Recently, several advances in the synthesis of colloidal semiconductor nanocrystals have been made, allowing for size and shape control.[14−19] Of particular interest in this respect is the ability to obtain quantum confined wurtzite CdSe nanorods with a narrow distribution of lengths and diameters. Well-characterized samples of CdSe nanorods have become a model system to study theories of quantum confinement; for instance, it has been demonstrated, both theoretically and experimentally, that they emit linearly polarized light along the *c*-axis[14] and that the degree of polarization is dependent on the aspect ratio of the particles.[20] Semiconductor nanorods are of particular interest because of their possible applications in light-emitting diodes,[21−23] in low-cost photovoltaic devices,[24−26] and their propensity to form liquid crystalline phases.[27]

In semiconductor quantum dots, high emission efficiency from band-edge states is required if we want to study in detail their electronic structure or, more practically, if they are to be used as emitters in any application. Unfortunately, the band-edge emission from nanocrystals has to compete with both radiative and nonradiative decay channels, originating from surface electronic states. In colloidal nanocrystals, coating the surface of the nanocrystals with suitable organic molecules can minimize this problem. The judicious choice of a passivating agent can, in fact, improve the size-dependent band-edge luminescence efficiency, while preserving the solubility and processability of the particles.[28] Unfortunately, passivation by

* To whom correspondence should be addressed. E-mail: alivis@uclink4.berkeley.edu.

(1) Bawendi, M. G.; Steigerwald, M. L.; Brus, L. E. *Annu. Rev. Phys. Chem.* **1990**, *41*, 477−496.
(2) Murray, C. B.; Norris, D. J.; Bawendi, M. G. *J. Am. Chem. Soc.* **1993**, *115*, 8706−8715.
(3) Alivisatos, A. P. *Science* **1996**, *271*, 933−937.
(4) Brus, L. *J. Phys. Chem. Solids* **1998**, *59*, 459−465.
(5) Heath, J. R. *Acc. Chem. Res.* **1999**, *32*, 388−388.
(6) Eychmuller, A. *J. Phys. Chem. B* **2000**, *104*, 6514−6528.
(7) Bruchez, M.; Moronne, M.; Gin, P.; Weiss, S.; Alivisatos, A. P. *Science* **1998**, *281*, 2013−2016.
(8) Alivisatos, A. P. *Sci. Am.* **2001**, *285*, 66−73.
(9) Schlamp, M. C.; Peng, X. G.; Alivisatos, A. P. *J. Appl. Phys.* **1997**, *82*, 5837−5842.
(10) Klimov, V. I.; Mikhailovsky, A. A.; Xu, S.; Malko, A.; Hollingsworth, J. A.; Leatherdale, C. A.; Eisler, H. J.; Bawendi, M. G. *Science* **2000**, *290*, 314−317.
(11) Weller, H. *Angew. Chem., Int. Ed.* **1998**, *37*, 1658−1659.
(12) Harrison, M. T.; Kershaw, S. V.; Burt, M. G.; Rogach, A. L.; Kornowski, A.; Eychmuller, A.; Weller, H. *Pure Appl. Chem.* **2000**, *72*, 295−307.
(13) Chan, W. C. W.; Nie, S. M. *Science* **1998**, *281*, 2016−2018.
(14) Peng, X. G.; Manna, L.; Yang, W. D.; Wickham, J.; Scher, E.; Kadavanich, A.; Alivisatos, A. P. *Nature* **2000**, *404*, 59−61.
(15) Manna, L.; Scher, E. C.; Alivisatos, A. P. *J. Am. Chem. Soc.* **2000**, *122*, 12700−12706.
(16) Peng, Z. A.; Peng, X. G. *J. Am. Chem. Soc.* **2001**, *123*, 1389−1395.
(17) Jun, Y. W.; Lee, S. M.; Kang, N. J.; Cheon, J. *J. Am. Chem. Soc.* **2001**, *123*, 5150−5151.
(18) Jun, Y. W.; Jung, Y. Y.; Cheon, J. *J. Am. Chem. Soc.* **2002**, *124*, 615−619.
(19) Pinna, N.; Weiss, K.; Urban, J.; Pileni, M. P. *Adv. Mater.* **2001**, *13*, 254−258.
(20) Hu, J. T.; Li, L. S.; Yang, W. D.; Manna, L.; Wang, L. W.; Alivisatos, A. P. *Science* **2001**, *292*, 2060−2063.
(21) Colvin, V. L.; Schlamp, M. C.; Alivisatos, A. P. *Nature* **1994**, *370*, 354−357.
(22) Duan, X. F.; Wang, J. F.; Lieber, C. M. *Appl. Phys. Lett.* **2000**, *76*, 1116−1118.
(23) Duan, X. F.; Huang, Y.; Cui, Y.; Wang, J. F.; Lieber, C. M. *Nature* **2001**, *409*, 66−69.
(24) Huynh, W. U.; Peng, X. G.; Alivisatos, A. P. *Adv. Mater.* **1999**, *11*, 923−927.
(25) Brabec, C. J.; Sariciftci, N. S.; Hummelen, J. C. *Adv. Funct. Mater.* **2001**, *11*, 15−26.
(26) Gratzel, M. *Nature* **2001**, *414*, 338−344.
(27) Li, L. S.; Walda, J.; Manna, L.; Alivisatos, A. P. *Nano Lett.*, in press.

10.1021/ja025946i CCC: $22.00

means of organic molecules is often incomplete or reversible, exposing some regions of the surface to degradation effects such as photooxidation.[29,30] In some cases, chemical degradation of the ligand molecule itself or its exchange with other ligands might lead to unstable and therefore unusable nanocrystals.[30]

In the case of colloidal CdSe nanorods, there are two additional factors that might further reduce the luminescence from band-edge states, when compared to spherical CdSe nanocrystals. In nanorods, the surface-to-volume ratio is higher than that in spheres, and this increases the occurrence of surface trap-states. In larger dots, the increased delocalization of carriers reduces the overlap of the electron and hole wave functions, lowering the probability of radiative recombination. The delocalization of carriers should be particularly high in a nanorod, where they are free to move throughout the length of the rod, thereby leading to reduced luminescence in nanorods.

To efficiently and permanently remove most of the surface states of the nanocrystal, an inorganic material can be epitaxially grown on its surface,[31−39] in analogy with the well-developed techniques for the growth of 2D quantum wells.[40−44] A stringent requirement for the epitaxial growth of several monolayers of one material on the top of another is a low lattice mismatch between the two materials. If this requirement is not met, strain accumulates in the growing layer, and eventually may be released through the formation of misfit dislocations, degrading the optical properties of the system.[35]

In the case of "spherical" colloidal CdSe nanocrystals, there are two methods of efficient inorganic passivation, one by means of a spherical layer (or shell) of ZnS[34,35] and the other by means of a shell of CdS.[36] The choice of these materials is based on the fact that both ZnS and CdS provide a potential step for electrons and holes originating in the nanocrystals, reducing the probability for the carriers to sample the surface. Surprisingly, the requirement for a low lattice mismatch is not as stringent as for 2D systems, because the total area over which the strain accumulates is small, and the total strain energy at the interface can remain below the threshold for inducing dislocations. The extended surface of the CdSe rods has an average curvature that is intermediate between the surface of a spherical dot and that of a flat film. In addition, since CdSe nanorods can be produced with lengths ranging from a few nanometers to a hundred nanometers, the coherent growth of an epitaxial shell over a region that is much more extended than the surface of a spherical dot is more challenging. Both conditions imply that interfacial strain will play a much more important role in rods than in dots. An additional issue that must be taken into account is the solubility of the resulting particles. The shell growth must be carried out in a surfactant that provides surface accessibility for the shell material to grow, while preventing aggregation of the particles. The temperature must also be kept low enough to prevent nucleation of the shell material, while high enough that the surfactant is dynamically going on and off the nanocrystal surface allowing access to the monomers.[35]

In this report, we demonstrate the growth of a CdS/ZnS graded shell grown on CdSe rods, in the presence of a small amount of Cd precursor in trioctylphosphine oxide at low temperature (160 °C). The CdS is more likely to grow initially since its lattice mismatch with CdSe is less than that of ZnS. This layer of CdS mediates the growth of the more highly strained ZnS, but the luminescence of the core/shell nanocrystals is not increased very much. The shell growth is uniform and epitaxial, completely coating the CdSe core, but it may have defects present due to the lower growth temperature. After a photochemical annealing process, the resulting shell increases the luminescence efficiency of nanorods from below 1% to up to 20−25%, while preserving their solubility in a wide range of solvents. Further, these CdSe rods offer an excellent opportunity to study the evolution of strain in nanostructures.

Experimental Section

I. Materials. Dimethylcadmium ($Cd(CH_3)_2$, 97%) and tri-*n*-butylphosphine ($C_{12}H_{27}P$ or TBP, 99%) were purchased from Strem. $Cd(CH_3)_2$ was vacuum distilled and stored at −35 °C under argon. Selenium (Se) (99.999%), tri-*n*-octylphosphine oxide ($C_{24}H_{51}OP$ or TOPO, 99%), diethylzinc ($C_4H_{10}Zn$, or Et_2Zn, 1.0 M solution in heptane), and hexamethyldisilathiane ($C_6H_{18}Si_2S$ or $(TMS)_2S$) were purchased from Aldrich. Hexylphosphonic acid ($C_6H_{15}O_3P$ or HPA 99%) was purchased from Organometallics Inc., and tetradecylphosphonic acid ($C_{14}H_{31}O_3P$ or TDPA, 98%) was purchased from Alfa. All solvents used were anhydrous, purchased from Aldrich, and used without any further purification.

II. Stock Solutions. Stock solutions were prepared in a drybox under Ar and then placed in a refrigerator at −20 °C. For the synthesis of CdSe nanorods, we prepared the solution for each precursor separately. For the Se precursor, selenium powder was dissolved in TBP (concentration of Se 7.79 wt %). For the Cd precursor, $Cd(CH_3)_2$ was dissolved in TBP (concentration of Cd 32.29 wt %). The stock solution for the ZnS shell was prepared by dissolving 152 mg of $(TMS)_2S$ and 0.63 g of the Et_2Zn solution in 4.1 g of TBP. In this solution the Zn:S molar ratio is 1:1. The stock solution for the CdS/ZnS graded shell was prepared by mixing 0.5 g of the Et_2Zn solution, 37 mg of a solution of $Cd(CH_3)_2$ in TBP (32.29 wt %), and 76 mg of $(TMS)_2S$. The resulting solution was then diluted in 2.05 g of TBP. In this solution the Zn:Cd:S molar ratio is 1:0.12:0.63.

III. Synthesis of CdSe Rods. All manipulations were performed using standard air-free techniques, unless otherwise stated. In a typical synthesis, a mixture of HPA, TDPA, and TOPO[20] was degassed at 120 °C for 1 h in a 50 mL three-neck flask connected to a Liebig condenser, after which 0.5 g of the Cd precursor solution was added dropwise. The resulting mixture was then heated to 360 °C, and 2.5 g of the Se precursor solution was quickly injected. After injection, the temperature dropped to 290 °C and was maintained at this level throughout the synthesis. When desired, the synthesis was stopped by removing the

(28) Talapin, D. V., R. A. L.; Kornowski, A.; Haase, M.; Weller, H. *Nano Lett.* **2001**, *1*, 207−211.
(29) Katari, J. E. B.; Colvin, V. L.; Alivisatos, A. P. *J. Phys. Chem.* **1994**, *98*, 4109−4117.
(30) Aldana, J.; Wang, Y. A.; Peng, X. G. *J. Am. Chem. Soc.* **2001**, *123*, 8844−8850.
(31) Spanhel, L.; Haase, M.; Weller, H.; Henglein, A. *J. Am. Chem. Soc.* **1987**, *109*, 5649−5655.
(32) Hoener, C. F.; Allan, K. A.; Bard, A. J.; Campion, A.; Fox, M. A.; Mallouk, T. E.; Webber, S. E.; White, J. M. *J. Phys. Chem.* **1992**, *96*, 3812−3817.
(33) Eychmuller, A.; Mews, A.; Weller, H. *Chem. Phys. Lett.* **1993**, *208*, 59−62.
(34) Hines, M. A.; Guyot-Sionnest, P. *J. Phys. Chem.* **1996**, *100*, 468−471.
(35) Dabbousi, B. O.; RodriguezViejo, J.; Mikulec, F. V.; Heine, J. R.; Mattoussi, H.; Ober, R.; Jensen, K. F.; Bawendi, M. G. *J. Phys. Chem. B* **1997**, *101*, 9463−9475.
(36) Peng, X. G.; Schlamp, M. C.; Kadavanich, A. V.; Alivisatos, A. P. *J. Am. Chem. Soc.* **1997**, *119*, 7019−7029.
(37) Kershaw, S. V.; Burt, M.; Harrison, M.; Rogach, A.; Weller, H.; Eychmuller, A. *Appl. Phys. Lett.* **1999**, *75*, 1694−1696.
(38) Cao, Y. W.; Banin, U. *J. Am. Chem. Soc.* **2000**, *122*, 9692−9702.
(39) Haubold, S.; Haase, M.; Kornowski, A.; Weller, H. *ChemPhysChem* **2001**, *2*, 331−334.
(40) Herman, M. A.; Sitter, H. *Microelectron. J.* **1996**, *27*, 257−296.
(41) Beanland, R.; Dunstan, D. J.; Goodhew, P. J. *Adv. Phys.* **1996**, *45*, 87−146.
(42) Dunstan, D. J. *J. Mater. Sci.: Mater. Electron.* **1997**, *8*, 337−375.
(43) Ledentsov, N. N.; Ustinov, V. M.; Shchukin, V. A.; Kop'ev, P. S.; Alferov, Z. I.; Bimberg, D. *Semiconductors* **1998**, *32*, 343−365.
(44) Shchukin, V. A.; Bimberg, D. *Rev. Mod. Phys.* **1999**, *71*, 1125−1171.

Table 1. CdSe Core Nanorod Growth Conditions and Corresponding Average Sizes

rod length (nm)	rod diameter (nm)	HPA (g)	TDPA (g)	TOPO (g)	reaction time (min)
18	5.0	0.04	0.46	3.50	5
23	3.3	0.13	0.34	3.55	2
21	3.3	0.08	0.39	3.53	4
36	4.5	0.13	0.34	3.55	5

heating mantle and by rapidly cooling the flask. In the present series of experiments, we prepared four samples of CdSe rods of different lengths and aspect ratios by varying the relative concentration of TOPO:HPA:TDPA and the growth time. The details are reported in Table 1.

After cooling the solution to 50 °C, 4.0 mL of methanol was added to precipitate the rods from the solution. This suspension was then transferred to a drybox, where it was centrifuged, and the precipitate was washed three times with methanol. The final precipitate was then dried under Ar and stored in the drybox. Because of the high degree of uniformity of the rods that this synthesis procedure yields, no further size selective precipitation was carried out on any samples.

IV. Epitaxial Growth of CdS/ZnS Graded Shell. Five grams of TOPO was placed into a 50 mL three-neck flask, pumped under vacuum at 120 °C for 20 min, and then cooled to 60 °C. Ten milligrams of dry nanorods was dissolved in 2.0 mL of chloroform. This solution was removed from the glovebox and injected into the TOPO solution at 60 °C. The chloroform was removed by pumping the mixture under vacuum for 20 min. The temperature of the mixture was raised to 160 °C. Depending on the desired thickness of the shell, a given amount (see Table 2) of the CdS/ZnS stock solution was loaded into a syringe and injected dropwise into the flask. A typical injection rate for this series of experiments was around 0.1 mL/min. After the injection was completed, the solution was kept at 160 °C for 10 min. During this time, the shell growth was completed. The temperature in the flask was then lowered to 40 °C, and 3.0 mL of octanol was added to quench the unreacted precursors. The resulting solution was immediately transferred under Ar into the glovebox and stored in the dark.

V. Precipitation and Redissolution of Core/Shell Rods. The solution of nanocrystals in TOPO/TBP/octanol was stable, optically clear, and no precipitate was observed even several months after the synthesis. Addition of methanol to this solution caused the precipitation of the nanocrystals, which could then be easily redissolved in solvents such as chloroform, toluene, or tetrahydrofuran. There were a few cases in which the core/shells did not redissolve. To avoid this problem, we found it was very effective to add a small amount (1 mg/mL) of a phosphonic acid, such as hexylphosphonic (HPA) acid, or of an amine such as hexadecylamine (HDA). In this case, after methanol was added, the solution immediately turned turbid, and the collected precipitate could then be readily redissolved. Solubility problems were also encountered when a precipitate (obtained without the addition of HPA or HDA) was washed several times with methanol. Here the addition of HPA or HDA to the solvent caused the immediate redissolution of the particles. Henceforth we will call these samples "HPA-capped" and "HDA-capped" nanorods, respectively. This is to distinguish them from samples of nanorods precipitated and redissolved without the assistance of additional surfactants, which will be called "TOPO-capped" nanorods.[45,46] In addition, we will call "raw nanorods" the samples obtained by simply diluting in chloroform the original solution of nanocrystals in TOPO/TBP/octanol, without any precipitation or redissolution procedures.

VI. Characterization of Samples. All sampling procedures for the optical characterization of the samples were carried out under Ar unless otherwise stated. In the case of CdSe nanorod cores, a small amount of sample (~0.2 mL) was removed via syringe from the flask before the shell growth. In the case of core/shell nanorods, a small amount of the final solution stored in the drybox (~0.2 mL) was used; depending on the particular experiment, this solution was processed according to one of the procedures described in the previous section. The sample was diluted to an optical density of between 0.1 and 0.25 by addition of anhydrous chloroform in a glovebox.

A. UV−Vis Absorption Spectroscopy. Absorption spectra were measured using a Hewlett-Packard 8453 UV-visible diode array spectrometer equipped with a deuterium lamp having a resolution of 1.0 nm.

B. Photoluminescence Spectroscopy. Photoluminescence (PL) spectra were recorded on a Spex 1681 0.22m/0.34m spectrometer. PL quantum efficiencies of the nanorods in chloroform were calculated by comparing their integrated emission to that of a solution of Rhodamine 6G in methanol. Optical densities of all solutions were adjusted to between 0.1 and 0.25 at the excitation wavelength to avoid reabsorption effects. The excitation wavelength used for all measurements was 480 nm. Emission spectra were corrected for the wavelength-dependent response of the photomultiplier tube and for the refractive indexes of methanol and chloroform.

C. Photochemical Shell Annealing. Laser irradiation experiments to photochemically anneal the shells were carried out by exposing a 1 cm path-length quartz cuvette filled with a diluted solution of CdSe nanorods or CdSe/CdS/ZnS core/shell nanorods to a continuous Ar^+ laser (Lexel 95 ion laser, Lexel Laser, Inc.). The power of the laser was tuned between 50 and 120 mW, depending on the particular experiment. The 457.9 nm and the 514.5 nm line were alternatively used as excitation lines. The laser spot on the sample had a diameter of approximately 1 cm. The number of nanoparticles in the cuvette was estimated by evaluating the average weight of a single nanorod and the total amount of CdSe in the solution. By measuring the laser power absorbed by the nanocrystal solution, it is possible to calculate the average number of photons absorbed by each particle per second of exposure to the laser light.

D. Transmission Electron Microscopy. Nanocrystal size, morphology, and structure were measured via TEM. At the National Center for Electron Microscopy at Lawrence Berkeley National Laboratory, a Topcon EM002B electron microscope was used. The microscope was operated at an accelerating voltage of 120 kV. At the UC − Berkeley Electron Microscope Lab, a FEI Tecnai 12 was used with an operating voltage of 120 kV.

Nanocrystals were deposited from dilute solution onto a 3−4 nm thick film of amorphous carbon supported by 400 mesh copper grids (purchased from Ted Pella). One drop of nanocrystal solution in chloroform was deposited onto the grid and evaporated.

Structural determination was accomplished using high-resolution TEM (HRTEM) at 550 000× magnification. Average sizes and morphologies were measured at 140 000× magnification, calibrated using known crystal lattice spacings. Average lengths and shape distributions were determined by counting at least 200 nanocrystals per sample for statistical purposes.

E. EDX. Energy-dispersive X-ray spectroscopy (EDX) was performed using a Philips CM200/FEG at the National Center for Electron Microscopy at Lawrence Berkeley National Laboratory. This microscope was operated at an accelerating voltage of 200 kV using an Oxford Model 6767 energy-dispersive X-ray detector with an energy resolution of 1.36 eV for Mn Kα radiation. Between 20 and 100 nanorods were used per scan, and at least 10 scans were taken per sample. The average scan time was between 20 and 40 min. For composition determination, scans times of the same length were used, and EDX scans were normalized to the Se Kα line.

F. Powder X-ray Diffraction. Powder X-ray diffraction was performed on a Bruker-AXS D8 general area detector diffraction system (GADDS), using Co Kα radiation (1.79026 Å). Two-dimensional patterns were angle integrated to obtain the patterns displayed. The

(45) Despite the use of this notation, some of the original TOPO molecules remain on the nanorod surface after surfactant exchange.
(46) Kuno, M.; Lee, J. K.; Dabbousi, B. O.; Mikulec, F. V.; Bawendi, M. G. *J. Chem. Phys.* **1997**, *106*, 9869−9882.

Table 2. Core/Shell Nanorod Growth Conditions, Final Average Sizes, Number of Shell Monolayers, and Composition of the Shell

sample	mL of shell stock solution	rod length (nm)	rod diameter (nm)	no. of shell monolayers	CdS in shell	Zn:Cd in shell
core	0	22.8	3.3	0	0%	NA
thin shell	0.6	24.2	4.4	2	35%	2:1
medium shell	0.75	27.0	6.0	4.5	22%	4:1
thick shell	1.5	29.8[a]	7.3	6.5	22%	4.5:1

[a] The given length is the average "body" length and does not include the tail if present.

instrument resolution is 0.07° in 2θ, and the accumulation time for each frame of each sample was 20 min. Three frames were taken per sample, centered at 2θ angles of 25°, 40°, and 55°, and at Ω angles of 12.5°, 20°, and 27.5°, respectively. XRD samples were prepared by evaporating a concentrated nanocrystal solution on a quartz plate. Prior to the measurements, the samples were washed with methanol to remove excess organic material and then dried. All peaks were fit using commercial software (PeakFit v4) utilizing a Gaussian*Lorentzian peak shape.

Results

I. Epitaxial Growth of a CdS/ZnS Graded Shell. Initial attempts to grow a ZnS shell on the nanorods used syntheses developed for shell growth on spherical nanocrystals. The results varied from nucleation of ZnS nanocrystals to the growth of thin shells (less than one monolayer) with irregular lumps. We determined that the large lattice mismatch between CdSe and ZnS was preventing thicker shell growth. To remedy this, small amounts of $Cd(CH_3)_2$ were added to the stock solution to facilitate growth of a CdS layer. CdS has a lattice spacing between that of CdSe and ZnS, which decreases the overall strain in the system. In the stock solution used for this series of experiments, the Zn:Cd ratio was quite high (~8:1), to promote the growth of ZnS, using the CdS only as an intermediate between the CdSe and the ZnS. The Zn:S molar ratio was set higher than 1:1 to ensure a Zn-rich surface. This allows the phosphine oxide, which specifically binds to metal sites, to easily coordinate the surface of the nanocrystals. Upon gradual injection of the stock solution, a color change from dark red to brown was observed. The degree of color change was dependent on the nanocrystal sample and on the amount of stock solution added. In the following experiments, the amount of stock solution injected ranged from 0.25 to 1.5 mL.

II. Structural Characterization. The thickness of the CdS/ZnS shell was controlled by the amount of precursor injected. We use several techniques, including direct and indirect methods of observation, to monitor and characterize the shell's thickness, structure, crystallinity, and composition. Figure 1 shows low-resolution TEM images of a CdSe core nanorod (3.3 × 22.8 nm) (a), the same cores with a thin shell (b), a medium shell (c), and a thick shell (d). In these images one can see the increase in diameter of the nanorods from 3.3 nm in the cores to 4.4 nm in the thin shell sample, 6.0 nm in the medium shell sample, 7.3 nm in the thick shell sample. This corresponds to growing roughly 2, 4.5, and 6.5 monolayers of CdS/ZnS shell for the thin, medium, and thick shell samples, respectively. The shell is observed to be very regular and conforms to the shape of the underlying CdSe core as long as the shell is less than 5−6 monolayers thick. This is true not only for the medium length rods shown in Figure 1, but is observed to be independent of aspect ratio as seen in Figure 2. In fact, the shell growth seems to improve the overall regularity of the rods in that they seem to be straighter than the cores themselves (the irregularities in the cores are caused by zinc blende stacking faults in them).[15] This does not hold true for the thickest samples, however. As

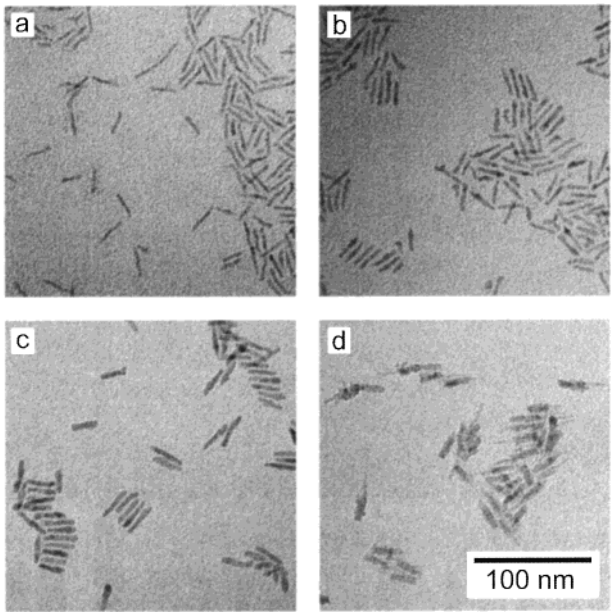

Figure 1. Transmission electron micrographs (TEMs) of the medium length (3.3 × 23 nm) CdSe core nanorods (a) and the same cores with different thickness shells of CdS/ZnS (b−d). The shell thickness is 2 monolayers (b), 4.5 monolayers (c), and 6.5 monolayers (d).

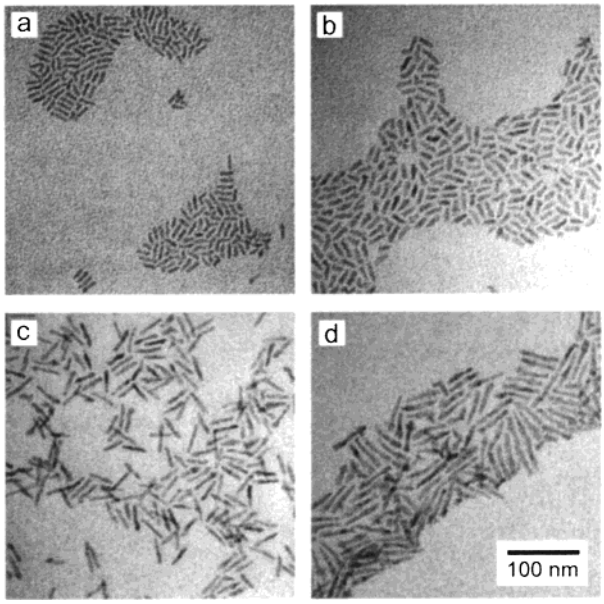

Figure 2. Transmission electron micrographs (TEMs) of the short (5.0 × 18 nm) CdSe core nanorods (a) and the same cores with a CdS/ZnS shell (b). TEMs of the long (4.5 × 36 nm) CdSe core nanorods (c) and the same cores with a CdS/ZnS shell (d).

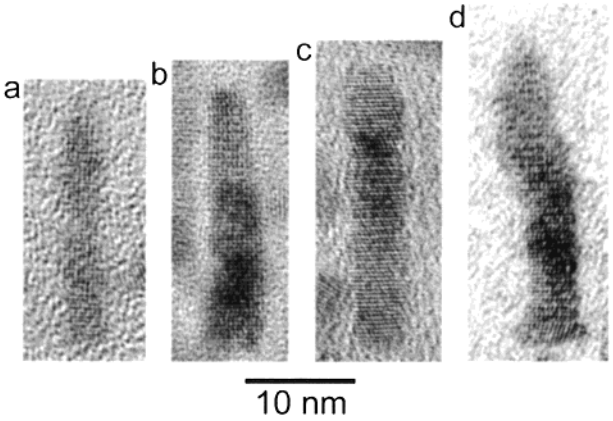

Figure 3. High-resolution transmission electron micrographs (HRTEMs) of the medium length (3.3 × 23 nm) CdSe core nanorods (a) and the same cores with different thickness shells of CdS/ZnS (b−d). The shell growth is epitaxial with fringes going through both core and shell. The shell growth is also regular except for the thickest sample (d) where the strain of the ZnS becomes too great and is relieved by irregular growth of ZnS on the shell.

seen in Figure 1d, once past a certain shell thickness, a tail is observed to grow straight out of one end of the rods, and the overall surface of the rods becomes rough. It is important to note that separate nuclei of CdS or ZnS particles were not observed via TEM in any of our samples.

In addition to the above, TEM, HRTEM, and XRD were used to determine the structure and crystallinity of the core/shell structures. In Figure 3, the HRTEM images of the medium length nanorod cores (a), the same cores with a thin shell (b), medium shell (c), and thick shell (d) of ZnS are shown. The lattice fringes are continuous through both the core and the shell implying epitaxial growth of the shell. There were no obvious stacking faults or defects observed at the interface of core and shell. In addition, the core and shell both have a wurtzite structure, and they increase in both diameter and length as the shell thickness increases, although the length increases slightly faster than the diameter. The thickest shell samples, where the growth of a ZnS tail is observed, are more difficult to image in the HRTEM. At low magnifications, with a large beam spot size, the thin tails can be clearly observed (Figure 1d), but when the spot size is decreased at higher magnifications (∼550 kX) the tails are damaged by the beam faster than an image can be taken.

Powder X-ray diffraction patterns of the same samples are shown in Figure 4. The bulk pattern of CdSe (Figure 4a) matches exactly that of the CdSe nanorod cores with the exception of the relative intensities of the peaks. The sharp 002 peak (29.6° 2θ) results from the extended crystalline domain along the *c*-axis of the wurtzite lattice. As the shell is grown and its thickness increases, the diffraction peaks shift toward smaller *d*-spacings (larger 2θ). This means that the growth of the CdS/ZnS shell is compressing the lattice planes in the CdSe core and that the compression increases as a function of shell thickness. Since a CdSe rod is an anisotropic system (in both crystal structure and shape), we should expect this compression to have a different effect on the various families of planes of the crystal. The shifts of different diffraction peaks in samples with increasingly thicker shells are shown in Table 3.

The diffraction patterns from the thin and medium thickness shell samples show that, apart from the aforementioned shifts,

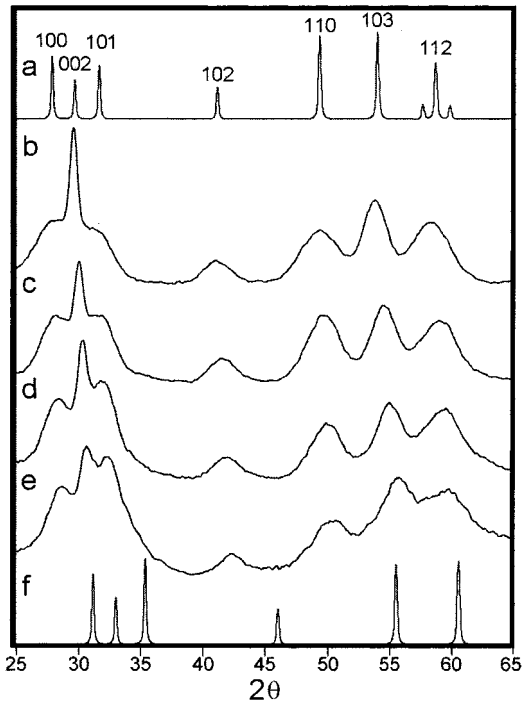

Figure 4. Powder X-ray diffraction (XRD) of the medium length (3.3 × 23 nm) nanorod cores (b) and core/shells (c−e). The bulk XRD pattern of CdSe (a) and ZnS (f) is given for reference. The initial XRD pattern of the CdSe core nanorods (b) matches the peak positions of bulk CdSe, but the intensities are different. The 002 peak is very narrow and more intense than the other peaks because of the extended domain along the *c*-axis of the nanorods. In the thin (c) and medium (d) shell samples, all of the peaks shift, and the intensity of the 002 peak decreases relative to the other peaks. In addition to following the aforementioned trends, the thick shell sample (e) displays some small broad peaks corresponding to the ZnS growths and tails observed on them in the TEM.

Table 3. XRD Peak Changes as a Function of Shell Thickness

sample	002 peak position	002 *d*-spacing change	100 peak position	100 *d*-spacing change
core	29.6	0.0%	28.1	0.0%
thin shell	30.05	1.5%	28.4	0.9%
medium shell	30.35	2.4%	28.6	1.5%
thick shell	30.75	3.7%	28.75	2.0%

the peak widths are almost unchanged as compared to the core spectrum and that no additional peaks are present. In the thickest sample though, the peaks have broadened significantly, and there may be small broad diffraction peaks that overlap with the ZnS bulk peaks (Figure 4f). Once tails have begun growing on the rods, they diffract as if they were small domains of isolated ZnS. Because of Debye−Scherrer broadening, they are observed as very broad peaks with low intensity.

To determine the shell composition, EDX spectroscopy was used. Again, the same four samples characterized by TEM, HRTEM, and XRD were analyzed. All of the spectra were normalized to the Se Kα line since the amount of Se in the cores and core/shells remains constant. The lines used are shown in Figure 5. It is clear that there is no Zn or S in the CdSe core nanorods. As the shell thickness increases, the amount of these elements present in the shell also increases. The Cu line is due to scattering in the microscope off the Cu TEM grid and was subtracted when determining the area of the Zn Kα line. Since we are also adding Cd, the amount of Cd also increases with increasing shell thickness as seen in the Cd Lα and Lβ spectra.

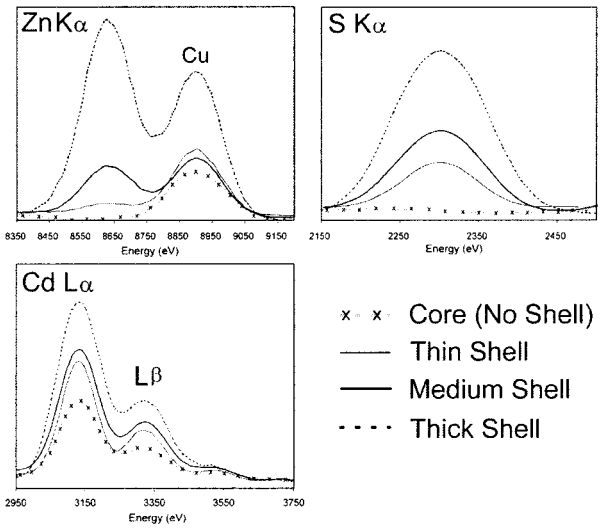

Figure 5. Energy-dispersive X-ray (EDX) spectra of the medium length (3.3 × 23 nm) nanorod cores and core/shells. The Se Kα spectrum is not shown as it was used for normalization of all the samples, and it does not differ between them. The Cu Kα line was subtracted when calculating the Zn Kα area. It is very clear that there is no Zn or S in the core nanorods. The amount of these elements increases as a function of shell thickness. The Cd L lines are present in the initial CdSe core sample but also increase as a function of shell thickness due to the growth of CdS in the shell.

Combining the EDX data with the sizes collected via TEM, the composition of the shell was determined as a function of shell thickness. CdS makes up 35% of the shell in the thin shell sample, 22% of the shell in the medium shell sample, and 22% of the shell in the thick shell sample. Since the thin shell sample has slightly less than two monolayers of shell grown on it, this corresponds to about $^2/_3$ of a monolayer of CdS, the remainder being ZnS. As the thickness increases, the CdS continues to grow, but the ratio of Zn:Cd increases as seen in Table 2.

III. Optical Characterization and Photochemical Annealing. The significant red shift in the absorption and emission spectra from core/shell samples also confirms that a relevant percentage of the shell is composed of CdS. Given the small energy difference between the bottom of conduction bands in CdSe and in CdS (0.2 eV in the bulk limit), the photogenerated electrons in colloidal CdSe/CdS dots can easily tunnel from the CdSe cores into the CdS shell (the core electrons have to overcome a potential step of 0.55 eV). When the thickness of the CdS shell increases, the absorption and luminescence spectra of CdSe/CdS dots shift to lower energies, since the confinement energy for the electrons is lower.[35] This effect is less remarkable in CdSe/ZnS dots, where the potential barrier for both carriers to tunnel from the CdSe cores into the ZnS shell is approximately 0.9 eV, but a red shift is still expected.[35]

Figure 6 shows the absorption spectra (solid line) of CdSe core nanorods, and the same cores with two different thickness shells. The solutions were "raw", as described in paragraph V of the Experimental Section. In the core−shell samples, there is a progressive red shift in the spectral features, with respect to the starting CdSe cores, as the thickness of the shell increases. This suggests that CdS is included in the shell, since a less remarkable shift would be expected from a core−shell system with only ZnS in the shell. The cores had a luminescence quantum yield (QY) lower than 1%, the thin shell sample had a QY of 4%, and the QY of the medium shell sample was again less than 1%.

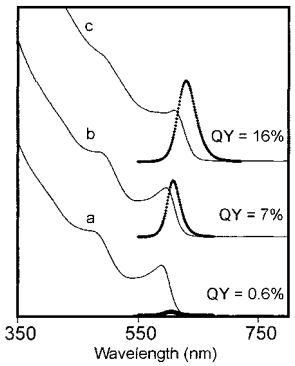

Figure 6. Absorption spectra (solid line) of medium length (3.3 × 21 nm) CdSe core nanorods (a) and thin (b) and medium (c) core/shell samples. Photoluminescence (PL) spectra (broken line) of the same samples after photoannealing. The absorption spectra do not change upon photoannealing.

The same figure shows the emission spectra of the three samples (dotted lines) after exposure to laser light overnight.[47] The QY from the thin shell sample increased to 7%, whereas the QY from the medium shell sample increased to 16%. Further exposure to laser light did not affect the QY from the core/shell samples. On the other hand, the same laser treatment on the CdSe cores did not significantly increase their QY. In fact, their luminescence either remained constant or decreased during laser irradiation. In all samples, the laser treatment did not cause any relevant spectral shift in absorption or luminescence, or any change in the optical density of the nanocrystal solutions; this rules out any possibility that the shell grew or shrank during laser illumination. In addition, TEM, HRTEM, and XRD were carried out on samples before and after illumination. No noticeable shape change was observed. We refer to this laser-induced increase in photoluminescence QY in core−shell rods as "photochemical annealing" or "photoannealing".

An increase in luminescence was observed in all core/shell samples that were photoannealed. Solutions of nonannealed core/shell rods kept under dark had low QY, even several weeks after the synthesis. After photoannealing for a few hours, their QY increased without any spectral shift. Figure 7a shows the measured QY for a CdSe core sample and core/shell as a function of the average number of photons absorbed per particle. The core/shell sample was raw.[48] The nanorods in the CdSe core sample had a length of 21 nm and a diameter of 3.3 nm. In the core/shell sample, the ZnS shell was 2.5 monolayers thick. The core/shell sample underwent photochemical annealing as its QY started from 3% and saturated at 17%, whereas the QY from the core sample remained less than 1%.

To check the influence of the postsynthesis treatment on the photochemical annealing, the above experiments were repeated on the same core/shell sample, but cleaned according to the procedures described in paragraph V of the Experimental Section. Three additional samples were then prepared from the original TOPO/TBP/octanol solution: TOPO-capped, HPA-capped, and HDA-capped core/shell. All these samples displayed quantum yield enhancement following photochemical annealing, although the HDA-capped sample reached the highest QY (it started at 4% and increased to 21%), the HPA-capped sample

(47) The exposure time of these samples was 20 h on average. The exciting wavelength was 514.5 nm, the laser power was approximately 80 mW, and the optical density of all solutions was 0.2 at 480 nm.
(48) Note: this core/shell nanorod sample could be easily precipitated from the original solution and then redissolved without the addition of HPA or HDA.

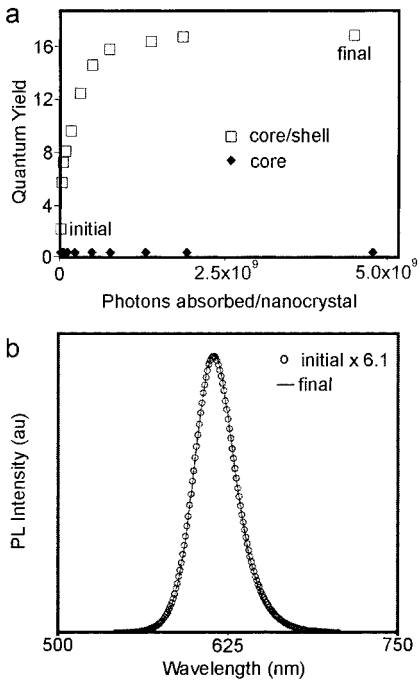

Figure 7. QY of medium length (3.3 × 21 nm) CdSe core nanorods (◆) and medium core/shell (□) samples as a function of photons absorbed/nanocrystal (a). The cores do not change significantly with time, but the core/shell's QY increases significantly after absorbing ~10^9 photons/nanorod and then remains constant. Two PL spectra from the same core/shell sample are shown in (b). The initial, nonphotoannealed sample (○) was multiplied by 6.12 to match the intensity of the final photoannealed sample (−). There are no noticeable changes in the peak shape, peak maximum, or full width at half maximum after photoannealing the sample.

experienced the lowest increase in QY (from 3 to 8%), and the TOPO-capped sample went from 2 to 11%. We also checked the effect of laser exposure on the CdSe nanorod cores capped with HDA.[49] After overnight laser exposure, the HDA-coated CdSe nanorod cores experienced a degradation in their QY (from 4 to 2%).

All laser exposure experiments were repeated using the 457.9 nm laser line excitation. For the core/shell rods, the QY versus photons absorbed per particle showed the same behavior as in the previous experiments, saturating after the same number of absorbed photons, whereas CdSe cores again experienced either no change or a decrease in QY. This indicates that the photoannealing process is not dependent on the excitation wavelength, as long as that wavelength is absorbed by the nanocrystal. In all cases, the QY of the photoannealed core/shells was much higher than the initial, preannealing value. More importantly, this process is irreversible; all cleaned samples of photoactivated core/shell nanocrystals, left in the dark under Ar for months, did not increase or decrease their QY by significant amounts (less than 5% variation was considered to be within the experimental error). In addition, there is no change in the fluorescence peak shape or peak maximum over this period of months. This is true for all of the surfactant-exchanged core/shells and core/shells that were washed with methanol at least once to remove any unreacted precursors, any unreacted precursors, before photoannealing. The only sample that showed any change over time was the raw core/shell nanorods. After photoannealing, this sample underwent a very slow degradation process, most likely due to the presence of reactive species in the solution. Given the lower stability of raw core/shell nanorods, all quantitative studies were carried out on surfactant-exchanged or cleaned core/shell samples.

IV. Photostability of the Core/Shell Rods. The solutions of photoactivated core/shell nanorods (obtained as described in the previous section) were opened to air and exposed again to laser light to check their stability against photooxidation. During these experiments, every nanocrystal in each sample absorbed approximately 3.5×10^9 photons over 8 h.[50] The HDA-capped sample showed the highest stability, with no change in QY and no blue shift in the luminescence peak. The HPA-capped and the TOPO-capped samples both experienced a blue shift of approximately 10 meV (4 nm) in their PL peak. The QY from the TOPO-capped sample slightly decreased (from 11 to 10%), whereas the PL from the HPA-capped sample increased (from 8 to 14%). The corresponding cores oxidized more under the same conditions.

Discussion

The growth of highly luminescent core/shell nanorods elucidates three basic concepts in interfacial growth: when both ZnS and CdS precursors are added, CdS preferentially grows first to reduce the interfacial energy; photoannealing permanently changes the core/shell nanorods, implying a structural reorganization; and growing shells on nanorods allows for the study of strain in a system that is intermediary between a "0D" nanocrystal core and a "2D" bulk surface.

Interfacial segregation is required for shell growth in this system. We add all of the shell precursors simultaneously, and yet CdS grows first on the CdSe core. Although the ratio of Zn:Cd injected is ~8:1, the ratio of ZnS:CdS in the first two monolayers of shell is only 2:1. As the shell thickness increases, this ratio goes from 2:1 to 4:1 to ~4.5:1 and levels out as the shell thickness increases. While mixed semiconductor shells have been grown before,[51] this is the first case that we are aware of in colloidal nanocrystal core/shell growth of spontaneous interfacial segregation. The concentration of Zn in the precursor solution cannot compensate for the larger ZnS lattice mismatch, so initially Cd is more likely to stick to the surface of the CdSe cores. The farther away from the core (or the thicker the shell), the more the ratio depends solely on the concentration. When no Cd is added, the strain is so great that either no shell grows at all or a tail of ZnS grows out one end of the nanorods.

This interfacial segregation could also be partially driven by the lower solubility of CdS with respect to ZnS in the surfactant used to grow the shell (TOPO). This concept of selective precipitation has been used to grow CdS/HgS/CdS quantum dot/quantum wells in aqueous solvents due to the large difference in solubility products of Cd^{2+} and Hg^{2+}.[33] It is known that Cd atoms form less stable complexes with TOPO than Zn atoms do,[52] and this may influence the order in which the atoms add to the core nanorod surface. If the shell growth were purely

(49) To prepare amine-coated CdSe rods, the cores were dissolved in chloroform in the presence of a small amount of HDA (1 mg per mL of solution), and the solution was stirred for 1 day to promote ligand exchange with the amine.

(50) In this series of experiments, the optical density of all solutions was adjusted to 0.1 at 480 nm. The laser power was ~120 mW, and the excitation wavelength was 514.5 nm. The samples were exposed for 8 h to the laser light.

(51) Micic, O. I.; Smith, B. B.; Nozik, A. J. *J. Phys. Chem. B* **2000**, *104*, 12149−12156.

due to solubility differences, then it might be possible to grow a pure ZnS shell on CdSe core nanorods. However, this is not observed because the strain between CdSe and ZnS is too large. Therefore, we believe that the main mechanism responsible for the formation of graded shells in our system is strain-induced interfacial segregation.

Interfacial segregation is necessary to grow a uniform epitaxial shell on the nanorods. Perhaps we could take advantage of this process to add precursors that would preferentially grow different types of shells on different faces of the core nanorods. This could be done by choosing materials with a lattice mismatch that would induce less strain on one crystal face than others. Another possibility would be to add more precursors, thereby growing multilayered, graded shells that would self-segregate based on the interfacial energy.

In a typical synthesis of core/shell dots, such as the CdSe/ZnS or the CdSe/CdS system, as the thickness of the shell increases, the luminescence QY first increases, and then declines. This trend is believed to be a consequence of increased strain in the shell.[35,36] As long as the strain can be tolerated, the epilayer passivates the interface trap states and does not create additional mid-gap states. Once past a certain shell thickness, the strain is released through the formation of dislocations in the shell. Dislocations act as nonradiative recombination centers and lower the QY. In our system, we noticed the same trend under normal conditions. However, after we irradiated our samples with laser light, the QYs increased significantly; even samples with a thick irregular shell had a QY greater than 10% after this process.

The low luminescence observed in samples before laser irradiation indicates that a significant amount of nonradiative recombination centers is present throughout the shell. There is a permanent increase in QY of our core/shell nanorods, after laser irradiation, suggesting that the laser induces a structural reorganization in the shell. The laser power was kept low enough that the temperature of the solution remained constant. In addition, experiments were performed where solutions of core/shell nanorods were externally heated to 160 °C, and the photoluminescence was monitored. Even after hours at this temperature, there was no increase in QY. This implies that a photochemical process is responsible for annealing the core/shells. Thermal annealing cannot be performed above the growth temperature of 160 °C since other processes such as Ostwald ripening or dissolution of the particles can occur.

Enhancement of luminescence in semiconductor quantum dots and films irradiated with low-power light has been previously observed. The most commonly encountered case is the increase of QY from nanocrystals upon exposure to light, in the presence of air.[53,54] In this case, the mechanism involved is either the adsorption of oxygen and/or water molecules, which reduces recombination from surface states, or a surface photooxidation, which can create an additional barrier for the carriers. Prolonged exposure to light in the presence of oxygen inevitably results in photooxidation. This can be seen readily by the decrease in particle size and a corresponding blue shift in the PL spectra.[30,55]

In several systems, a reversible increase in luminescence is observed under light irradiation above the band gap.[56−59] This process involves the saturation of surface trap states by photogenerated carriers and is usually called "photobrightening". The effect is usually observed at low temperatures, where the activation energy for detrapping of the carriers is considerably higher than the thermal energy. Trapped carriers can be re-excited to the conduction band by an activated "detrapping process", via absorption of another photon.[60] The brightening effect is temporary, and once the light source is turned off or the sample is heated, the carriers are slowly detrapped, with a consequent decrease in band-edge emission. In semiconductor nanocrystals embedded in a host matrix, such as a glass or polymer, an increase in luminescence can also derive from photoionization of crystals and carrier capture by the host.[61] Ionization of nanocrystals is believed to be enhanced by Auger processes,[62,63] since their probability of occurrence in nanocrystals is higher due to the breakdown of translational symmetry and the higher overlap of the carrier wave functions.[64,65]

Neither of the aforementioned mechanisms is probably responsible for the laser-induced increase in QY that we observe in our core/shell nanorods. The increase in QY cannot be ascribed to photooxidation processes, or to the absorption of oxygen or water molecules at the surface of the nanocrystals, for several reasons. Oxygen and water have been carefully excluded in all laser irradiation experiments. In addition, photooxidation causes a blue shift in the optical spectra due to a decrease in particle size. Such a blue shift has never been observed in our experiments. In fact, if the PL spectra of core/shell nanorods before and after laser irradiation are scaled to the same height, there is no difference between the two. The peak maximum, peak shape, and full width at half maximum all remain constant. Photobrightening and Auger-induced charging of the nanocrystals are not the active mechanisms in our samples because they are reversible processes. Photoionization effects would lead to a red shift in the spectra, which is not observed in our samples after annealing. The QY from annealed core/shell rods remains high even after they have been in the dark for several months. Not only does the QY remain higher than in the nonannealed samples, but also it remains constant within the experimental error.

Structural changes that lead to a permanent change in the luminescence QY of semiconductor dots or films are known to occur under high-power laser excitation, although there are

(52) Dyrssen, D.; Liljenzin, J. O.; Rydberg, J. *Solvent Extraction Chemistry*, Proceedings of the international conference held at Gothenburg, Sweden, August 27−September 1, 1966; North-Holland Pub. Co.: Amsterdam, 1967.
(53) Cordero, S. R.; Carson, P. J.; Estabrook, R. A.; Strouse, G. F.; Buratto, S. K. *J. Phys. Chem. B* **2000**, *104*, 12137−12142.
(54) Bol, A. A.; Meijerink, A. *J. Phys. Chem. B* **2001**, *105*, 10203−10209.
(55) van Sark, W.; Frederix, P.; Van den Heuvel, D. J.; Gerritsen, H. C.; Bol, A. A.; van Lingen, J. N. J.; Donega, C. D.; Meijerink, A. *J. Phys. Chem. B* **2001**, *105*, 8281−8284.
(56) Yu, J. Q.; Liu, H. M.; Wang, Y. Y.; Fernandez, F. E.; Jia, W. Y.; Sun, L. D.; Jin, C. M.; Li, D.; Liu, J. Y.; Huang, S. H. *Opt. Lett.* **1997**, *22*, 913−915.
(57) Oda, M.; Shen, M. Y.; Saito, M.; Goto, T. *Journal of Lumin.* **2000**, *87*−*9*, 469−471.
(58) Masumoto, Y.; Ogasawara, S. *J. Lumin.* **2000**, *87*−*9*, 360−362.
(59) van Dijken, A.; Meulenkamp, E. A.; Vanmaekelbergh, D.; Meijerink, A. *J. Phys. Chem. B* **2000**, *104*, 4355−4360.
(60) Heath, J. R.; Shiang, J. J. *Chem. Soc. Rev.* **1998**, *27*, 65−71.
(61) Masumoto, Y. *J. Lumin.* **1996**, *70*, 386−399.
(62) Krauss, T. D.; O'Brien, S.; Brus, L. E. *J. Phys. Chem. B* **2001**, *105*, 1725−1733.
(63) Chepic, D. I.; Efros, A. I.; Ekimov, M. G.; Ivanov, M. G.; Kharchenko, V. A.; Kudriavtsev, I. A.; Yazeva, T. V. *J. Lumin.* **1990**, *47*, 113−127.
(64) Kharchenko, V. A.; Rosen, M. *J. Lumin.* **1996**, *70*, 158−169.
(65) Gaponenko, S. V. *Optical Properties of Semiconductor Nanocrystals*; Cambridge University Press: Cambridge, 1998.

known cases where these changes occur under photoexcitation. For instance, disordered ZnS:Mn films showed enhanced luminescence from Mn^{2+} ions when irradiated by ultraviolet laser with energy pulses well below the conventional annealing threshold.[66] This was explained by the low energy of formation and diffusion of defects in disordered semiconductors. Although in core/shell rods the evidence brought by TEM and XRD results can rule out a highly disordered shell, a certain number of defects are likely present at the highly strained interface. There is the possibility that chemical bonds at the interface can rearrange or that defects can diffuse to the outer surface through a photochemically activated process. This is possible because the shell is only few nanometers thick. In addition, laser irradiation can induce surface reconstructions, which would decrease the number of surface trap states.

TEM, HRTEM, and XRD were performed on samples before and after photoannealing. There were no shape or structural changes observed using any of these methods. This is not surprising, however, considering the fact that all of these techniques rely on diffraction from planes of atoms and are not sensitive to the positions of individual atoms. As borne out by simulations,[67] these techniques are not sensitive to the surface atoms or the individual atoms at the interface of the core/shell nanocrystals. Any structural changes occurring at the surface or interface would therefore not be observed.

The surfactant dependence of the core/shell QY can be understood by considering that in this system the carriers are not completely localized in the core and can sample the outer surface of the rod. This explains why some surfactants (long chain alkylamines) increase the luminescence from core/shell nanocrystals[28] by neutralizing surface trap states, whereas other molecules (such as pyridine) decrease it. Bulky surfactants, such as TOPO, are not able to passivate all the metal sites on the surface and are therefore less efficient than alkylamines. A more uniform surface coordination, such as the one offered by alkylamines, also imparts a higher stability against photooxidation. Although in our case, the addition of different surfactants leads to different initial and final QYs, the annealing process followed the same behavior as a function of incident photons. If the increase in QY were the result of the surfactant reacting with the surface of the shell, then we would not observe the same behavior by different surfactants with different functional groups.

All of this evidence indicates that the photoannealing leads to a permanent change in the core/shell nanorods. Such a permanent change not only rules out photobrightening or oxidation as the cause of the increased QY, but also supports the theory that a structural rearrangement has occurred. Since there are no obvious changes observed in the HRTEM and XRD of the annealed sample, but the changes are permanent, the annealing is most likely only affecting the core/shell interface or the surface of the shell.

Core/shell nanorods provide a unique system for the study of strain in shell growth. Unlike in 2D epitaxial growth, the substrate (in this case the nanorod) is not fixed, so the lattice planes can actually be compressed by growth of the shell material. In addition, since this is a 1D system, some of the crystal faces behave more like those in a 2D system, while other faces behave more like the 0D surfaces of a highly curved spherical nanocrystal. The growth of shells with such a high lattice mismatch accentuates the induced strain, and XRD provides a means to observe the strain induced by the CdS/ZnS shell. All of the diffraction peaks shift to lower *d*-spacings (higher 2θ) as a function of shell thickness. Upon shell growth, the 002 peak shifts the most of any of the diffraction peaks (in all samples). Each plane in the (002) family of planes extends for only 3−4 nm. On the other hand, the 100 peak is generated by planes that are parallel to the *c*-axis. Each of these planes extends along the whole length of the rods, which is at least 3 to 8 times larger than the (002) planes in the nanorods. This peak shifts less than any other diffraction peak (in all samples) as a function of shell thickness. All of the other diffraction peaks shift by amounts that are intermediate between the shifts in the 002 and the 100 peaks. This implies that the planes extending along the diameter of the rod (or having a significant component along the diameter) are more compressed than planes extending along the length of the rod. This observation can be understood if one considers that, unlike traditional methods of shell growth where the substrate is fixed (bulk), the substrate in this case is thin enough that the shell can actually compress the lattice planes of the core. This compression of planes is more pronounced at their edges, near the core/shell interface. Since planes made up of very few atoms, such as the ones along the diameter of the rods, are more affected by this perturbation, their average *d*-spacing will change more than the extended planes with many atoms. These larger planes, such as the (100) planes, which extend along the length of the nanorod, may only be compressed at their ends, but not throughout the entire crystal length.

In addition, the intensity of the 002 peak decreases relative to the other peaks in the sample. This is not what one might expect since TEM analysis shows that the average length of the rods is increasing with shell thickness. The increase in length should make the 002 peak narrower and more intense as the domain size is increasing. Once we take into account the strain, however, these results make sense. As the compression of the 002 planes increases with shell thickness, this will cause a broader distribution of observed domain sizes, thereby spreading out the 002 peak and decreasing its intensity, while the other *d*-spacings and therefore peaks are not affected as significantly.

The growth of a tail of ZnS out of one end of the nanorods also provides evidence of the intense strain present in these particles. After 5−6 monolayers of shell are grown, the strain induced by the lattice mismatch is too great to continue regular shell growth. To relieve this strain, ZnS grows as a tail out of one end of the rod. Since the tail consists solely of shell material, it only feels the strain for the few monolayers that connect it to the body of the rod. The rest of the tail has the unstrained lattice parameters of ZnS. A similar situation occurs for the lumps that grow on the other faces of the rod (the reason that a tail only grows out of one side is due to the lack of inversion symmetry in the wurtzite structure and the higher energy of the $00\bar{1}$ face relative to the other faces[15]). This is observed not only in the TEM but also in the XRD pattern of the thick shell samples (Figure 4e). In that pattern, some small very broad peaks of ZnS are observed on top of the core/shell diffraction. These peaks result from the tails and lumps that are diffracting as if they were small isolated domains of ZnS.

(66) Kononets, Y. F.; Veligura, L. I.; Ostroukhova, O. A. *Semiconductors* **1998**, *32*, 491−494.
(67) Wickham, J. N.; Herhold, A. B.; Alivisatos, A. P. *Phys. Rev. Lett.* **2000**, *84*, 923−926.

Conclusions

Interfacial segregation and photoannealing are used to grow highly luminescent core/shell structures despite the large lattice mismatch of CdSe and ZnS. These processes should be of use when applied to other core/shell systems. Photoannealing may help produce other stable core/shell structures with constant luminescence, and may provide some insight into the quantum yields of core/shell systems in general. Interfacial segregation in colloidal nanocrystal systems allows for simultaneous injection of different precursors to spontaneously yield the desired product. In addition, the growth of shells on anisotropic shapes provides a unique opportunity to study the strain at the interface. Since we can vary both shell thickness and core aspect ratio, we can study the strain from nearly spherical nanocrystals to those with planes extended in one dimension. Such information should help further the study of interfaces as well as provide a practical method for using the size- and shape-dependent properties of nanocrystals even in highly strained systems.

Acknowledgment. This work was supported by the Department Of Defense Advanced Research Projects Agency (administered by USC, Award No. 066995) and the Director, Office of Energy Research, Office of Science, Division of Materials Sciences, of the U.S. Department of Energy under Contract DE-AC03-76SF00098. We thank the National Center for Electron Microscopy for the use of their TEMs and R. Zalpuri and G. Vrdoljak at the UC − Berkeley Electron Microscope Lab for their assistance and the use of their TEM. Thank you to David Zaziski for assistance with the optical measurements, setup, and helpful discussions. Thank you to Dr. Natalia Zaitseva and Ben Boussert for many inspiring discussions.

Supporting Information Available: Energy-dispersive X-ray spectra of nanorods (PDF). This material is available free of charge via the Internet at http://pubs.acs.org.

JA025946I